GEOPHYSICS

The big impact of small quakes on tectonic tremor synchronization

Gaspard Farge* and Emily E. Brodsky

Tectonic tremor tracks the repeated slow rupture of certain major plate boundary faults. One of the most perplexing aspects about tremor is that some fault segments produce strongly periodic, spatially extensive tremor episodes, while others have more disorganized, asynchronous activity. Here, we measure the size of segments that activate synchronously during tremor episodes and the relationship to regional earthquake rate on major plate boundaries. Tremor synchronization in space seems to be limited by the activity of small, nearby crustal and intraslab earthquakes. This observation can be explained by a competition between the self-synchronization of fault segments and perturbation by regional earthquakes. Our results imply previously unrecognized interactions across subduction systems, in which earthquake activity far from the fault influences whether it breaks in small or large segments.

INTRODUCTION

The seismic signal known as tectonic tremor was first observed and linked to slow ruptures at the edge of the locked zones of some of the largest faults on Earth about 20 years ago (1, 2). Tremor is correlated with slow slip in space and time (3–6) and thus provides a high-resolution image of slow slip events on the fault (7). Observations are now long enough in some regions to record the patterns in time and space of dozens of cycles of loading, rupture, and healing. It is therefore a tool to understand stress cycles on the most studied faults in the world based on observations just a few kilometers beneath the expected rupture areas of M8 to 9 earthquakes (8, 9).

Here, we use the term "tremor" in a general sense to refer both to the observed seismic phenomenon and the underlying slow ruptures that generate it, especially when discussing tremor synchronization. We will also assume that low-frequency earthquakes and tremor are seismic manifestations of the same phenomenon—a broad spectrum of slow slip variations—observed at different timescales and frequency bands (10, 11).

The long catalogs of tectonic tremor show clear segmentation of plate boundary faults based on the typical extent of tremor and associated slip episodes. Some segments activate with almost perfect synchrony, in migrating episodes spanning the full segment extent, sometimes on several hundreds of kilometers, and recurring in regular, long-period intervals. Within other segments, tectonic tremor occurs in frequent, smaller episodes that are uncoordinated in time and space. For instance, in Nankai (Fig. 1, A and D), the main Kii peninsula segment (135.5° to 136.5°E, 400 to 550 km along-strike) activates synchronously, with the largest (~150+ km) coherent episodes of the entire region, while the short segment directly to the East, in Tokai (136.5° to 138°E, 550 to 700 km) segment, exhibits a slightly less spatially synchronized activity. Even more notable, the short segment west of the Kii peninsula (135° to 135.5°E, ~350 km) activates in an almost fully desynchronized manner, in frequent small bursts which never cross over to neighboring segments. Those patterns of tremor activity show that the fault produces a range of rupture styles along-strike, with astounding stationarity in time and space. Although the

segmentation of the shallow parts of the megathrust that produce large earthquakes may not reflect the segmentation of the deep parts, the mechanisms that influence it are probably similar (12). Therefore, understanding the dynamic factors that control if deep fault segments break synchronously or one part at a time opens the way to future breakthroughs in predicting rupture extents on the fault.

The segmentation of tremor in subduction zones has been interpreted as emerging from structural factors, such as the geology of the overriding plate or the topography of the slab. Those properties then influence the frictional or hydraulic behavior of the interface, which are thought to be reflected in the characteristic patterns of tremor recurrence within each segment (12–14). In addition to these structural factors, we note that dynamic factors may also influence segmentation and the behavior of tremor in each segment. Near-field stresses on the fault can promote synchronization: As a patch slips, neighbors are pushed toward failure and large parts of the fault slip collectively (15). On the other hand, outside perturbations like nearby earthquakes could prematurely trigger or delay the initiation of slip of local fault patches and thus disrupt spatial synchrony. Here, we therefore introduce the possibility that the degree of spatial synchronization of tremor—how much fault breaks at the same time within the segment—could be related to the abundance of nearby crustal and intraslab earthquakes.

Tremor activity is known to be particularly sensitive to external forcings, such as transient stresses from tides or passing seismic waves of high amplitude from global, regional, or local events (16–22). In most regions that produce tremor, the study of dynamic triggering by passing seismic waves has been limited to large, distant earthquakes. However, there is no reason to believe that small earthquakes could not trigger nearby tremor sources to fail, if sufficient stresses were reached. Han et al. (23) showed that local triggering of tremor by small earthquakes occurs in Nankai: intraslab earthquakes with magnitudes as small as ~3 trigger tremor activity in the immediate vicinity (~15 km away) within about 10 hours of the earthquake.

Small earthquakes are much more frequent than large earthquakes, and their influence is more regionally limited. Their desynchronizing influence should therefore be stronger. Because of their high rate of occurrence, they define a stationary segmentation of dynamic stress disturbance, which has the potential to perturb the synchronization of local slow ruptures into regular patterns. If those effects were substantial enough relative to structural factors, then

Department of Earth and Planetary Sciences, University of California Santa Cruz, Santa Cruz, CA, USA.
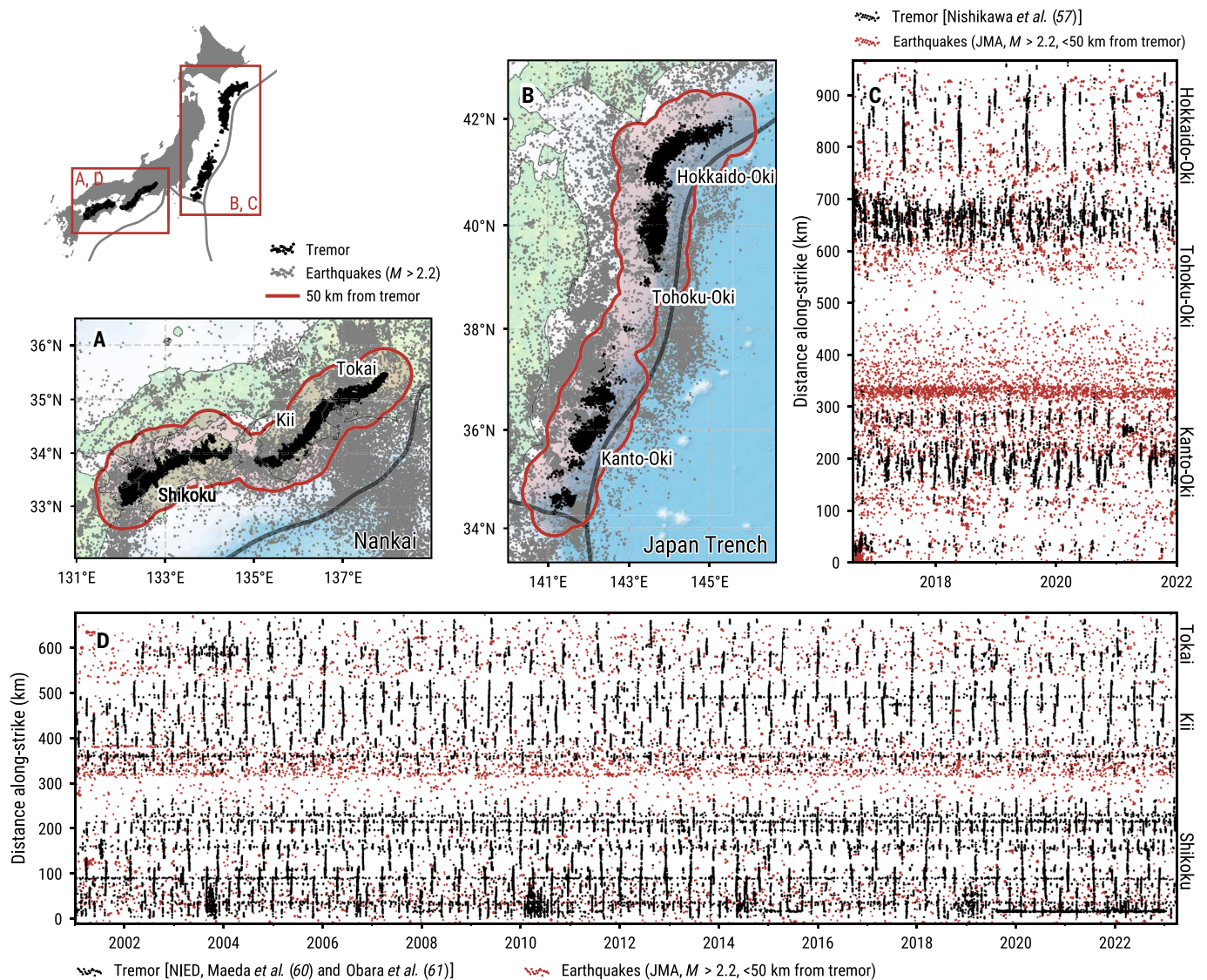*Corresponding author. Email: gafarge@ucsc.edu)

Fig. 1. Tremor synchronization patterns and earthquake activity in Japan. Maps of tremor (black) and earthquakes (gray) in (**A**) Nankai and (**B**) in the Japan Trench. Earthquakes are from the Japan Meteorological Agency (JMA) catalog with $M > 2.2$. The red contour indicates the area in which earthquakes are less than 50 km away from tremor. Time series of tremor and regional earthquake activity within 50 km of a tremor event in (**C**) the Japan Trench and (**D**) Nankai. Most of the regional earthquakes are not on the plate boundary but rather occur in the crust of the upper plate or within the slab. NIED is the Japanese National Research Institute for Earth Science and Disaster Prevention. More detailed information about data sources can be found in Table 1 and section S1 of the Supplementary Materials.

they could partly account for the absence or emergence of spatial synchronization of tremor activity within segments and perhaps even define those segments. In this work, we will assess whether the competition between tremor synchronization and perturbation from earthquakes is strong enough to be observed with the current state of tremor and earthquake catalogs and how important it is relative to structural factors in shaping tremor segmentation.

RESULTS
Tremor synchronization and earthquake perturbation in Japan
A first look at the tremor in Japan seems to confirm this proposition (Fig. 1). Segments with high earthquake ($M > 2.2$) activity near the tremor (events less than 50 km away from a tremor source) also seem to produce a less synchronized activity of tremor. Conversely, segments surrounded with lower earthquake activity appear to produce full-width ruptures. The most notable examples of highly synchronized segments with low perturbations from earthquakes include: in Nankai (Fig. 1D), 100 to 150 km (central Shikoku), ~200 km (East Shikoku), 400 to 500 km (Kii peninsula), and, to a lesser extent, 550 to 650 km (Tokai). In the Japan Trench (Fig. 1C), the northernmost segment 750 to 900 km (Hokkaido-Oki) is the most spatially synchronized and also the most isolated from small earthquake perturbation. On the other hand, the Western Kii peninsula (Nankai, ~350 km), North Tohoku-Oki (Japan Trench, 600 to 700 km), and North Kanto-Oki (Japan Trench, 250 to 300 km) are surrounded with high rates of seismicity, and the tremor activity within those

segments appears less spatially synchronized: The segments break in relatively frequent and complementary partial ruptures.

The Cascadia subduction zone is the only other zone in the world where tremor has been detected over decadal timescales and in a nearly continuous—although segmented—narrow band of 1400 km along-strike (Fig. 2). Cascadia has nearly a factor of 10 fewer earthquakes than Japanese subduction zones. It is also the region in the world where tremor episodes span the largest extent along-strike, up to several hundreds of kilometers in Central and Northern Cascadia. It should be noted that Southern Cascadia (Northern California, 100 to 300 km) displays the less synchronized activity of this region and is also surrounded by the hotspot of seismic activity in the Pacific Northwest, the Mendocino Triple Junction.

It appears that there exists an anticorrelation between the level of spatial synchronization of tremor and the rate of seismicity surrounding it. The relationship is seen both within a single subduction zone and in the comparison between different subduction zones. It could indicate that nearby small earthquakes locally affect the development of tremor patterns.

Measuring the relationship between tremor synchronization and regional earthquake activity

Encouraged by this initial observation, we now set out to systematically measure the relationship between tremor synchronization and the number of perturbations from earthquakes in several tremor zones around the world. We prefer to use regions that have a long enough record of activity as well as sufficient extent along-strike to allow us to accurately measure patterns of tremor synchronization along-strike. Worldwide, only the tremor zones of Cascadia, Nankai,

and the Japan Trench fit that description and allow us to investigate this relationship at the scale of the subduction zone. Given the limited range of the highest quality data, however, we also include data from Eastern Alaska (Alaska Peninsula subduction zone), New Zealand (Hikurangi subduction zone), California (Parkfield segment of the San Andreas fault), and Taiwan (Central Range fault) in our analysis to provide some global perspective and more generally compare tremor synchronization and perturbation from earthquakes region to region. In each of these regions, we select a catalog of tremor and one of earthquakes around the tremor, spanning the same period. For each tremor catalog, we check and sometimes model the depth location of tremor, define a strike direction, and trim off shallow sources. In addition, in Nankai, we test the dependence of catalog choices by analyzing two different tremor catalogs. The datasets used along with the parameters of this preprocessing step are summarized in Table 1 and in more detail in section S1 of the Supplementary Materials.

We count the number of earthquakes occurring during the analysis period closer than a threshold distance to each tremor event to understand the effects of intraslab and crustal seismicity on the intermittence of tremor. We test different distances of possible interaction (10, 20, 30, 50, and 100 km, in three dimensions). We count the total number of earthquakes above the maximum completeness (M2.2) of all the earthquake catalogs we are using in the vicinity of the tremor. Each tremor event location in the catalogs is considered as a potential tremor source and is thus associated with an activity rate for the zone around it. This is the activity that the tremor source and its associated slip patch "feel." We use the average annual number of earthquakes in proximity to the tremor sources in short, 10-km-long
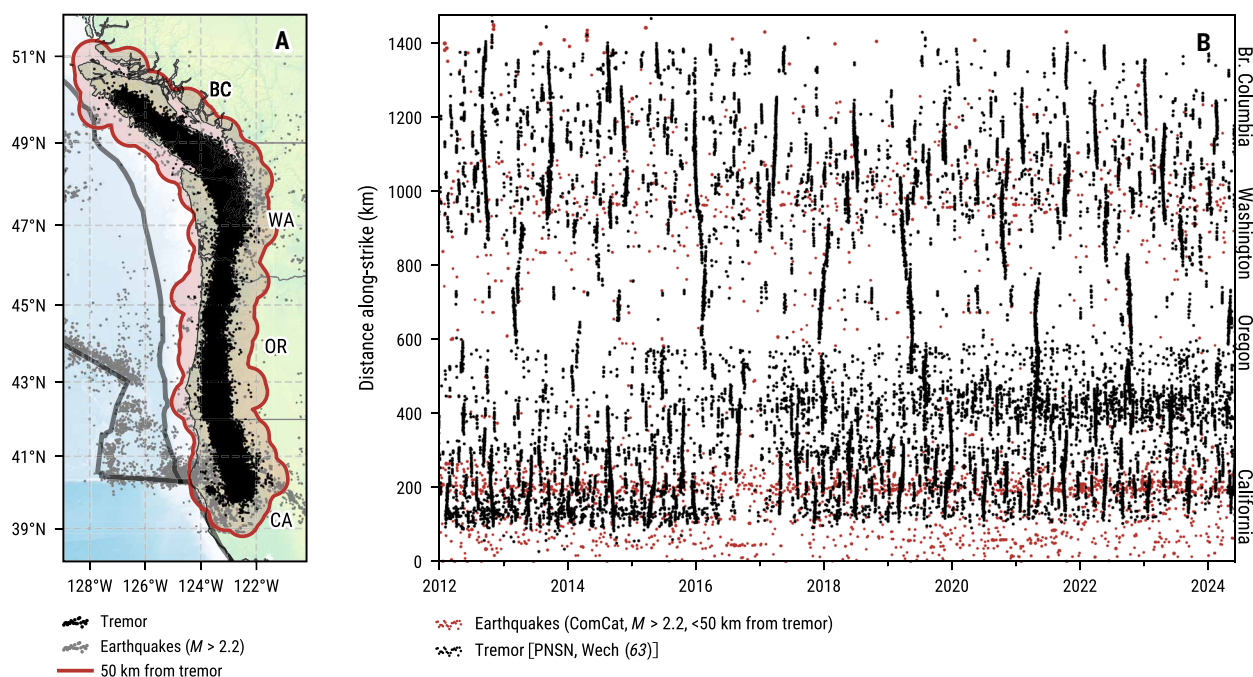
Fig. 2. Tremor synchronization patterns and earthquake activity in Cascadia. (**A**) Map of tremor (black) and earthquakes in the Cascadia subduction zone. Earthquakes are from the Advanced National Seismic System Comprehensive Earthquake Catalog (ComCat) catalog with $M > 2.2$. The tremor catalog is from the Pacific Northwest Seismic Network (PNSN). The red contour indicates the area in which earthquakes are less than 50 km away from tremor. (**B**) Time series of tremor and regional earthquake activity within 50 km of a tremor event. Most of the regional earthquakes are not on the plate boundary but rather occur in the crust of the upper plate or within the slab. Detailed information about data sources can be found in Table 1 and section S1 of the Supplementary Materials.

Table 1. Catalogs and datasets used in this study. Further details are in the Supplementary Materials.

Region	Tremor catalog	Earthquake catalog	Time span (mm/yyyy)	Along-strike extent	Depth model	Across-strike distance
Japan Trench	Slow-earthquake database (57, 58)[*]	JMA[*]	5.4 years (08/2016–01/2022)	860 km	(59)[*]	No trimming
Nankai	NIED[*] (60, 61)	JMA[*]	22.3 years (01/2001–04/2023)	700 km	(59)[*]	No trimming
Nankai	World Tremor Database[*] (48, 62)	JMA[*]	9 years (04/2004–04/2013)	700 km	Cataloged depth	50 km
Cascadia	PNSN[*] (63)	ComCat[*]	14.7 years (08/2009–06/2024)	1200 km	(41)[†]	100 km
Alaska	(24)[†]	ComCat[*]	2.8 years (01/2013–10/2015)	350 km	Slab2.0[*] (64)	No trimming
Hikurangi	(65)[†]	GeoNet[*]	6.8 years (01/2010–10/2016)	160 km	Slab2.0[*] (64)	No trimming
Parkfield	(66, 67)[*]	NCAeqDD[*] (68, 69)	16.6 years (06/2006–01/2023)	160 km	Cataloged	No trimming
Taiwan	(51, 70)[*]	CWASN[*]	10.9 years (01/2012–01/2023)	350 km	Cataloged	No trimming

[*]Datasets are available through queries on public websites. Detailed links and query parameters can be found in Materials and Methods. [†]Datasets are available in the Supplementary Materials of the cited publications.

segments along the plate interface as an estimate of the rate of perturbations—i.e., the number earthquakes felt by tremor sources in a year, averaged over a short segment. Results here use earthquakes $M > 2.2$ and within 50 km of tremor.

We quantify how synchronously a segment activates with its neighbors using a correlation length metric, which locally measures the characteristic size along-strike of the bursts that activate the considered region (see Materials and Methods). In a given tremor zone, we measure the synchronization of tremor along-strike using the same 10-km bins used for counting earthquakes. Figure 2 shows the results of this synchronization measure and earthquake counts for the Japanese tremor zones. It reproduces well visual estimates of both the synchronization size and its segmentation. The characteristic size we measure tends to be higher than just the average of all burst sizes that cross a segment. This is because longer bursts produce more tremor activity and thus weigh more in our correlation analysis than more frequent smaller bursts.

In Cascadia, Nankai, the Japan Trench, Eastern Alaska, Hikurangi, Parkfield, and Taiwan, we measure both the along-strike variation of correlation length and the along-strike variation of activity rate in the vicinity of the tremor zone, using the same method described above and the same set of parameters for all zones. Figure 3 shows the relationship between those measures along the strike of the Cascadia, Nankai, and Japan Trench subduction zones. Figure 4 shows a region-to-region comparison of tremor synchronization and earthquake perturbation across all zones. Figures detailing results for each zone can be found in the Supplementary Materials (figs. S2 to S9). As we are investigating very large-scale and time-averaged patterns, the sensitivity of our measures to the chosen catalog is low (figs. S3 and S4).

In individual regions long enough to analyze patterns along-strike (Fig. 3), the correlation length of tremor tends to be negatively correlated with the rate of nearby earthquake activity. As observed on the raw data (Figs. 1 and 2) and described in the previous section,

tremor appears to be less synchronized in segments where more earthquakes can affect the tremor loci. The anticorrelation between our measure of tremor synchronization and earthquake perturbation is very clear for tremor zones in Japan (Fig. 3). There, the correlation coefficients between the logarithm of tremor correlation length and the logarithm of the number of felt earthquakes are significantly negative $r = -0.4$ to -0.5, with a negligible chance of randomly occurring through sampling of uncorrelated variables ($P < 3 \times 10^{-3}$). A linear relationship between those properties would therefore explain $r^2 = 15$ to 25% of the variability of the synchronization observed in those zones. For the Cascadia tremor zone, the anticorrelation is much less clear ($r = -0.22$), although significant ($P = 0.02$). This should be expected: The number of earthquakes in the region is so low that their influence weighs less in comparison to structural factors, which probably define segment boundaries and the characteristics of tremor activity within those segments (12). For instance, the boundary between the Klamath and Siletzia terranes might be responsible of the relative desynchronization of tremor around ~400 km in Cascadia where the rate of perturbation from earthquakes is also relatively low (Figs. 2 and 3).

When compared region to region (Fig. 4), representative values of tremor correlation length and number of perturbing earthquakes in all the studied tremor zones clearly show an anticorrelation. Regions with more earthquake activity in the vicinity of the tremor zone develop less spatially synchronized tremor activity. There, especially above one M2.2 per year within 50 km, the correlation length L_{corr} looks like it cannot exceed an upper bound which is lower and lower with increasing number of perturbations N_{eq}, following a rough scaling of $L_{corr} \sim N_{eq}^{-0.5}$. Figure S10 in the Supplementary Materials demonstrates that this result holds best for a neighborhood of 50 km, but the trend is still obvious for all tested distances and for all sets of parameters (fig. S11)—although only specific sets of parameters lead to accurate estimates of tremor synchronization and perturbations from earthquakes (see section S2 of
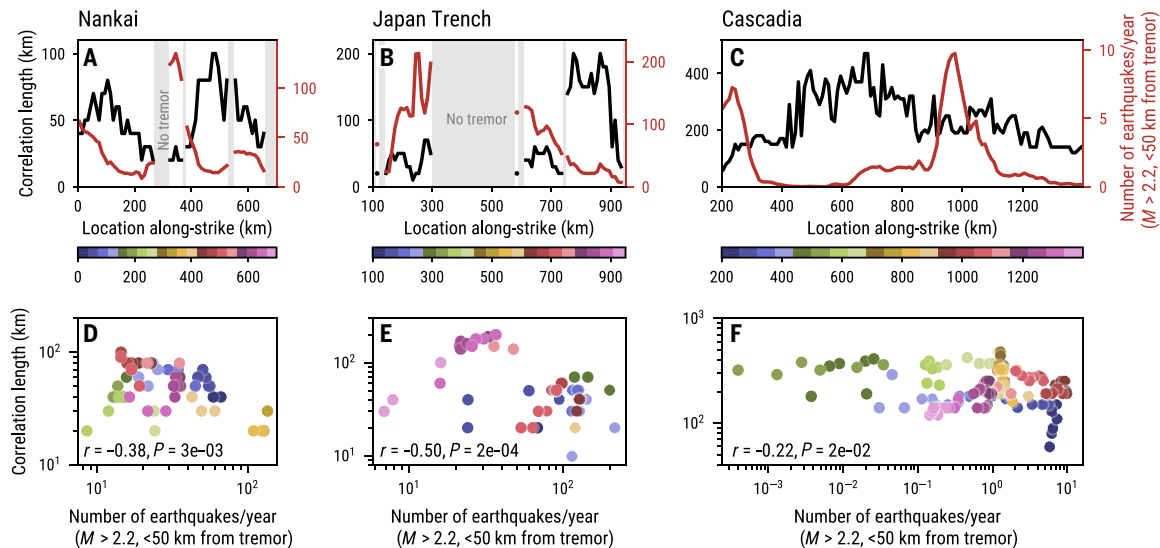
Fig. 3. Measures of tremor synchronization and perturbation by earthquakes. Tremor correlation length (black) and average annual number of earthquakes felt by tremor sources (in red) in bins of 10 km along-strike in (**A**) Nankai, (**B**) the Japan Trench, and (**C**) Cascadia. Earthquakes "felt" by tremor are $M > 2.2$ and within 50 km of a tremor source. Grayed out portions of the plot do not have enough tremor to trust the measurements. Relationship between tremor correlation length and number of earthquakes felt by tremor sources in (**D**) Nankai, (**E**) the Japan Trench, and (**F**) Cascadia. Pearson's correlation coefficient r between the logarithms of the two measures is shown on the plot, along with its P value. Dots are colored according to their location along-strike.
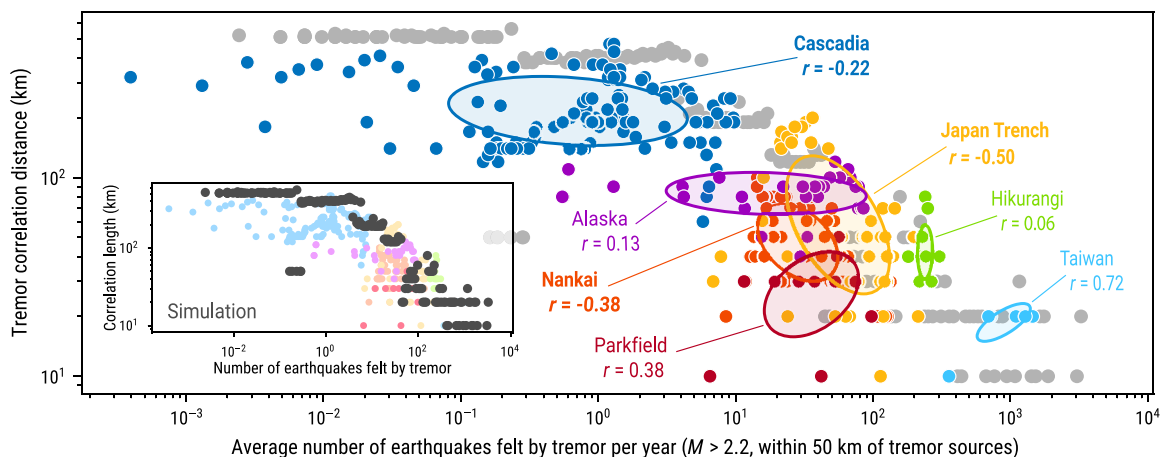

Fig. 4. Relationship between tremor synchronization and external perturbation by earthquakes. Measure of tremor synchronization and rate of perturbation by small earthquakes from observations in seven tremor zones. We count perturbations as the average number of earthquakes per year experienced by tremor sources in a spatial bin—$M > 2.2$, less than 50 km from the tremor source. For each region, we indicate Pearson's correlation coefficient r between the logarithm of the number of earthquakes experienced by tremor and the logarithm of correlation length. Regions where the correlation is significant ($P < 0.05$, see the main text for details) are annotated in bold font. Ellipses represent the central 60% of the point distribution in each region, to give a sense of the representative values for that region. The gray dots in the background and the inset graph shows the results of those measures on the simulated activity of randomly perturbed (synthetic earthquakes) pulse-coupled oscillators (synthetic tremor activity). Figure 5 describes the activity of this specific simulation in more detail. Detailed information about data sources can be found in Table 1 and section S1 of the Supplementary Materials.

the Supplementary Materials). The data in Cascadia define a clear plateau in Fig. 4: At low rates of surrounding seismicity, the relationship is weaker. This plateau seems to provide us with a lower bound for the significance of the perturbing effect of earthquakes on tremor synchronization—a seismicity rate of one M2.2 per year within 50 km.

The data in Alaska, Hikurangi, Parkfield, and Taiwan fall within the global pattern of Fig. 4, but the synchronization of tremor does not correlate with the local earthquake rate within each region

individually. There are good reasons for these regional limitations. In Hikurangi and Parkfield, the regions imaged by the catalogs are very narrow, limiting our ability to get a larger picture of the segmentation of tremor and thus making it hard to assess correlation. In Alaska, a slab tear and strong curvature are thought to be a major factor shaping tremor segmentation (24, 25) that appears to outweigh dynamic interactions. In Taiwan, the structure of the thrust fault that is hypothesized to host the tremor might be far less continuous than subduction megathrust and thus control a lot of the

patterns we observe. Those complications limit our interpretation of how patterns of synchronization can develop along-strike within each zone, in response to local perturbations to earthquake activity. They however still allow us to compare the representative values of synchronization that can exist with a given rate of earthquake activity. Under this more general lens, the overall alignment of segments of different zones in Fig. 4 is notable.

The most notable and robust feature of Fig. 4 is the absence of points in the upper right quadrant of the plot: No zone develops wide scales of synchronization in high seismicity environments. This absence is consistent with our proposition that the frequent activity of small earthquakes disrupts tremor synchronization and thus prevents the emergence of long-range correlation along-strike when the rate of perturbations from earthquakes is high.

Modeling the competition between tremor synchronization and earthquake perturbations

The competition between internal forces pushing toward synchronization and external perturbation can be reproduced in a simple model of those interactions and qualitatively matches our results (Fig. 4). We describe the self-synchronizing activity of tremor using a population of pulse-coupled oscillators connected in a line. The stress at each oscillator (tremor slip patch) is monotonically loaded, and when it reaches a threshold, it fires (tremor activity). The coupling is pulsatile. When an oscillator fires, its neighbors' charge is increased by a fixed amount, which can bring them to fire. Under undisturbed loading conditions, such pulse-coupled oscillators reach perfect synchronization almost regardless of initial conditions. This model framework has been used to explain the synchronous firing of biological oscillators, as cardiac muscle fibers or firefly populations (26). We add a limited amount of oscillator heterogeneity to model structural factors of segmentation (see Materials and Methods and fig. S12 for model details).

This model is similar to models that have been used to describe how fault elements interact to produce the complexity of sizes of earthquake activity (27–29) and slow earthquake activity (30–32). We chose to use a pulse-coupled oscillator system because of its simplicity: It describes interactions in a very simple and general manner which will allow us to add and study perturbations from nearby earthquakes in a similarly simplified fashion. In addition, the original description of the model includes a stress leakage term in the loading dynamics of oscillators [e.g., (26)]. This is a key feature that simulates stress leaking out of the fault as it loads toward failure. Leakage thus produces a concave curvature of the stress accumulation with time (Fig. 5A). Such leakage in the late phase of the stress cycle of ordinary friction earthquakes is inferred from observations of preyield in stick-slip experiments [e.g., (33) and Fig. 2] and is thought to be an important phenomenon in the tremor zone, where mechanical stresses are progressively released as the fault loads through viscous or otherwise distributed deformation (34, 35). The leakage term also reproduces aspects of fault-valving dynamics: Fault strength is progressively eroded by fluid pressure accumulation, at a slower and slower rate as the fluid pressure loading the fault leaks out, resulting in an asymptotic convergence toward failure [e.g., (13)]. The concavity of the stress loading curve is essential for the emergence of synchronization. It allows oscillators to be near failure for a longer time than when loading linearly (26). In the fault, it makes fault patches very sensitive to interactions and perturbation and thus more prone to triggering and synchronization. In addition to having a physical basis in the loading dynamics we expect for tremor sources, this simple loading dynamics is therefore consistent with the high sensitivity of tremor to external forces and the exceptional synchronization it can display.

The effect of perturbations from earthquakes is modeled by randomly perturbing oscillators, with a random stress pulse much weaker than the inter-oscillator coupling. Pulses are randomly positive
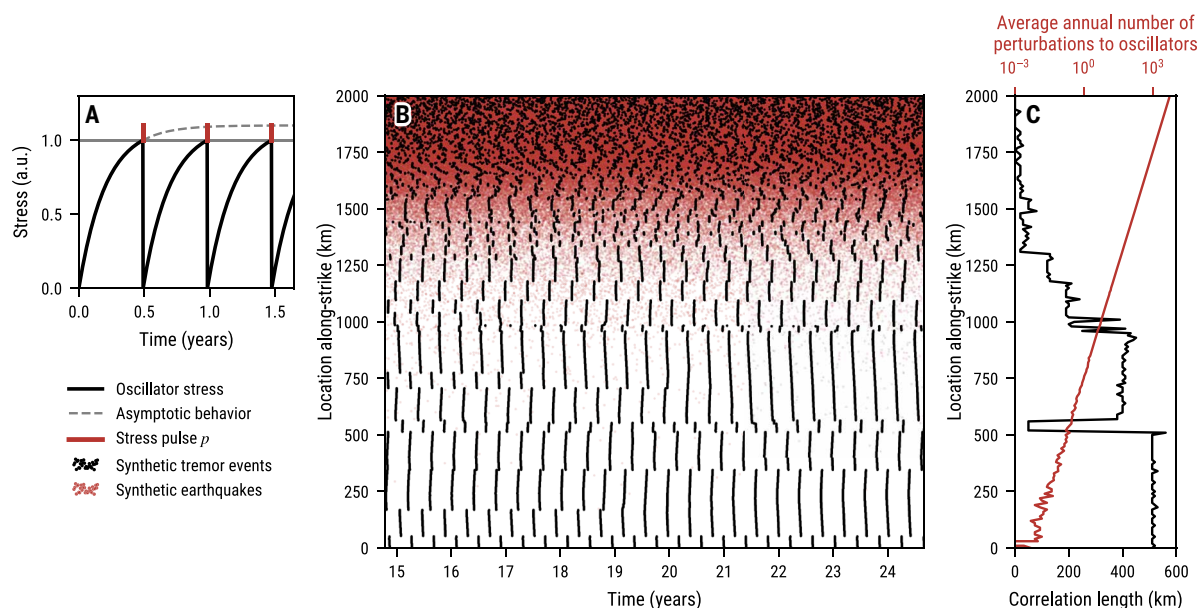

Fig. 5. Simulation of pulse-coupled oscillators (synthetic tremor activity) perturbed by external perturbations (synthetic earthquakes). (**A**) Stress cycles of an isolated oscillator, in arbitrary units (a.u.). (**B**) Simulated firing activity of pulse-coupled oscillators (simulated tremor, black dots), perturbed by external perturbations (simulated earthquakes, red dots). (**C**) Correlation distance of oscillator activity (black) and average number of perturbations per year (red), in non-overlapping, 10-km-wide segments along the simulation domain.

and negative, thus generating a small, random clock advance or delay to the model tremor sources. In this model, dynamic perturbations affect the state of stress and time to failure locally but do not necessarily result in instantaneous triggering, as can be observed from experiments and theory (36–38). For simplicity, they only perturb the model fault very locally, to simulate the effect of small nearby earthquakes which constitute most of the seismicity. Representative simulation results are shown in Fig. 5. We apply the same measure of synchronization as for real data and display the results along with real data on Fig. 4.

Just as in the real data, the oscillators with a lower rate of perturbation are able to synchronize on much longer segments, while a higher rate of external perturbation is associated with synchronization at a limited distance. This model captures the observation that the synchronization of tremor is affected by the activity of nearby small earthquakes. High rates of nearby earthquake activity send local stress perturbations which make the stress state at one oscillator different from that of its neighbors. It counteracts the synchronizing interactions by throwing off the phase alignment of the loading cycle of neighboring patches and thus breaks up local synchronization. Small portions of the fault that would otherwise synchronize with the rest of it are thus continuously pushed out of synchronicity by the perturbations and can sustainably produce small tremor bursts in perturbed segments (e.g., in Shikoku; Fig. 1D). This effect limits the characteristic size of tremor episodes, producing a more uncoordinated activity in space. The activity also seems to become less regular in time, as parts of a segment activate more independently. This can be seen in Fig. 5 (1000 to 1250 km) and when comparing segments of Kii and Tokai in Fig. 1D.

At low rates of nearby earthquake activity, the perturbations from earthquakes should be outweighed by more important, often structural factors. In Cascadia, for instance, earthquake activity competes with sharp lithological boundaries to define a segmentation (12), and only regions where the seismicity rate is high (more than a few $M > 2.2$ earthquakes within 50 km of tremor) are potentially influenced. In Alaska, the absence of an anticorrelation within the region could come from the fact that a complex slab tear seems to dictate most of the behavior of tremor (24), and only much stronger seismicity rates would be able to substantially weigh in. In simulations too, even the segments with low seismicity rate can show low correlation length and a segmentation (Figs. 4 and 5) because of the imposed underlying heterogeneity of the oscillators' loading cycles.

Last, a sudden increase of small earthquake activity near tremor should have a more or less immediate desynchronizing effect. Observing such a transient response in reality would be very direct evidence of the mechanism we argue is at play here—however, we have yet to find it: The activity of small earthquakes around tremor is remarkably stationary in Cascadia, Nankai, and the Japan Trench over the periods covered by the catalogs (Figs. 1 and 2).

DISCUSSION

These results seem to demonstrate that tremor activity, and by extension, the slow ruptures that it reflects evolve and are shaped in a complex, dynamic stress landscape. As noted above, tremor patterns have long been recognized to be influenced by structural factors. The geometry of the subduction zone, the topography of the plate, the lithology of the overriding plate, or thermo-hydro-mechanical properties at the plate interface all dictate how much stress can be

accumulated and how quickly and strongly it can be communicated to adjacent regions of the plate boundary. Those factors could also be responsible for causing the correlation we observe, making tremor less regular and more earthquakes in the same regions. Prior work has, for instance, shown that in Cascadia, tremor activity rates are spatially anticorrelated with crustal seismicity (39–41). Those studies proposed a common, external cause for this pattern—differential fluid migration pathways. Here, however, we propose that the correlation of tremor intermittence patterns with regional earthquake activity can be explained by dynamic interactions between tremor and earthquakes—the latter perturbing the former. The implication is that external stress perturbations originating in otherwise unconnected faults should play an important role in shaping tremor patterns.

Because the correlation we observe uses small earthquakes at a few tens of kilometers from the tremor loci, stresses are probably primarily transferred by seismic waves. Using empirical relationships (42), we can estimate that magnitude 1, 2, 3, and 4 earthquakes will respectively apply a stress on the order of 1 kPa to tremor sources of 2, 10, 45, and 200 km away—tidal and teleseismic stresses on the order of 1 to 10 kPa have been found to trigger tremor (17, 19). Through delayed triggering mechanisms (36–38), transient perturbations of a small fraction of the total stress drop could lead to permanent clock advance or delay in the loading cycle of slow slip patches. It is worth noting that a wide range of additional stress perturbations from tidal, oceanic, and atmospheric activity are present in Earth and have been shown to play a role in triggering tremor and slow slip (19, 43). Those stress transients and their distribution in space should also factor in the observed segmentation of rupture sizes at the depth of tremor.

Detecting tremor is a tricky business. Because of its emergent nature, tremor is hard to locate, especially at depth. It also resembles other sources of noise, e.g., trains, traffic, and rivers (44, 45). Its correlation in time with clear geodetic signals has been used to give more certainty of its tectonic origin (2). When the geodetic signals are expected to be too small, the episodic nature of sources are the only indices left of a tectonic source (46). As we have seen previously, however, the activity of nearby earthquakes should disturb episodicity, in addition to partly covering up tremor waveforms. This could explain the added difficulty of detecting tremor sources in areas with abundant crustal earthquakes, such as Taiwan, Chile, or New Zealand. Tremor has been detected there (47–51) but does not develop on large portions of the plate boundary faults and sometimes lacks a clear episodic recurrence, making it especially difficult to identify although those settings were, at first glance, perfect candidates to host tremor activity (52).

The relationships shown here suggest that the disturbance from repeated dynamic stresses of small earthquakes should also be considered in understanding the regularity of the recurrence of larger earthquakes in time and space. This problem is more complex, as the occurrence of smaller, more frequent perturbing earthquakes is strongly influenced by the activity of larger events. The investigation of interactions between frequent events and potential large earthquakes provides a way of estimating the stress landscape in which a large earthquake could develop, from the study of constantly occurring microseismicity.

In summary, we have shown an anticorrelation between earthquake rates and tremor synchronization that appears to partly explain geographic variations of tremor's spatial organization. Tremor naturally tends to synchronize in large segments but is often disturbed

by the earthquakes away from the plate boundary, resulting in more complex recurrence patterns in space and time. Earthquakes in the upper crust and in the interior of the slab are playing a major role in determining the megathrust activity in subduction zones. The observations presented here reveal a system-wide coupling between major faults and their seismic environment. The successful application of a simple conceptual model to this problem leads to exciting forecasting perspectives, potentially opening avenues to understand where faults can simultaneously rupture through hundreds of kilometers to produce large events.

MATERIALS AND METHODS
Preprocessing of earthquake and tremor catalogs
Details on where to find the catalogs used in the study—and which spatial and temporal bounds were used—can be found in the Supplementary Materials (section S1). In some cases, the depth location of the tremor events in catalogs is either not accurate or even not cataloged. In Cascadia, Hikurangi, and Alaska, we define the depth of each event as the depth of the slab interface directly below its cataloged horizontal location, using publicly available models of the slab interface at depth (see section S1 for the source of each slab model used). We fit a polynomial function to the epicentral locations of tremor to define the strike location used for the analysis. Events (earthquakes and tremor) are then projected onto this curve to define their along-strike location. In some cases, we exclude tremor events that are too far away from the along-strike curve defined by the deep tremor loci, in order not to bias the analysis by including too many earthquakes around shallower tremor sources. In Fig. 1A, the black dot cloud shows the locations of the trimmed tremor catalog along with the line defining the strike in transparent white.

Computing the correlation length
We use a correlation length as a measure of tremor synchronization, which estimates the spatial extent of the segment that activates coherently with a considered segment, or in other words, how large are the characteristic bursts that activate a given segment along-strike. Figure S1 illustrates details of how this measure is computed. In a given tremor zone, we segment the activity along-strike using the same 10-km bins used for counting earthquakes. We also investigate the robustness of the results to alternative binning sizes (fig. S11). The temporal activity of tremor within each 10-km bin is then represented as a time series of daily tremor counts (fig. S1, A and B). The activity counts of all segments are then cross-correlated with all other segments, over the duration of the available catalog. The maximum of the correlation function measures how strongly two segments interact with each other. For distant segments i and j, the maximum of the cross-correlation function is often located at nonzero lags, as the finite-speed migrations delays the correlation between segments. Because episodes of tremor migrate both from i to j and conversely from j to i, two maxima should be theoretically found at negative and positive lags corresponding to a given propagation velocity. As the information of both maxima are relevant for the correlation of activity between i and j, we therefore symmetrize the cross-correlation onto itself by averaging its values at positive and negative lags and locate the maximum value. To limit artifacts at long lags due to the correction of the bias of the cross-correlation of finite sequences, we only look for the maximum value at relatively short lags, corresponding to the time taken for migrations to cross the distance between segment i and j. We choose $V = 3.5$ km/day as the minimum migration speed considered to transfer meaningful information about activity from one segment to another. Considered lags are therefore contained between times 0 and d_{ij}/V, where d_{ij} is the distance separating segments i and j (fig. S1C).

This measure produces a modified cross-correlation matrix (fig. S1D), which catalogs the strength of temporal interactions between all possible pairs of segments C_{ij}. Although similar correlation matrices have been used in previous work to identify segments or sources that activate together in tremor zones (53–55), our modified correlation matrix allows to more accurately detect interactions by accounting for propagation delays and bidirectionality.

For each segment i, a synchronization length scale can be computed by measuring the distances in each along-strike direction to the furthest, well-correlated segment. Concretely, for a given segment i, we measure the off-diagonal extent along the j axis of the region where all values of C_{ij} are above a correlation threshold of 0.07. This summed correlation length measures the characteristic size along-strike of the bursts that activate segment i (fig. S1D). As cross correlations are performed on activity counts of each bin along-strike, more intense activation linked with the passage of longer bursts will make the measured size larger than a simple average of burst sizes. Figure 1C shows the results of this synchronization measure in Cascadia. It reproduces well visual estimates of both the synchronization size and its segmentation.

Perturbed pulse-coupled oscillator model
We model the synchronization of tremor using a population of coupled oscillators (26). The tremor source region is simulated by a one-dimensional line of 1000 tremor sources, spaced by 1 km each. Each source is progressively stressed according to the following evolution law

$$\frac{dy_i}{dt} = I - \alpha \times y_i(t)$$

where y_i is the stress state of a specific oscillator i, I is a stressing rate, α is a leakage rate, and all are positive quantities. We describe the relevance of the leakage term to model stress accumulation before slow slip in the last subsection of Results. We numerically solve this equation using a simple forward finite difference scheme for each oscillator. The stress undergone by each oscillator progressively increases, until it reaches $y_i = 1$. At that time, the oscillator "fires," and a synthetic tremor event is logged at position i. The charge of the firing oscillator is set to $y_i = 0$, and it starts a new loading cycle. Figure S9A describes the cycle of an isolated oscillator.

When an oscillator i fires, a pulse of charge p is added to the charge of its direct neighbors $i − 1$ and $i + 1$. Oscillators at each end of the line only communicate to one neighbor within the line—the boundary conditions are not cyclical. As oscillators fire, they bring their neighbor closer to firing, until all neighbors fire together, and the system reaches synchrony thanks to the pulsatile coupling. The period of the collective activation in this undisturbed system is the same as the oscillator's period, $T = −1/\alpha \times \log(1 − \alpha/I)$. We scale that period to 180 days (6 months) to reproduce similar timescales as in Nankai's tremor zone. Figure S9B displays the progressive synchronization and permanent activity of a line of N_x oscillators, with slight heterogeneity in the oscillators (see further).

Numerically, we only check for firing events $y_i > 1$ once during a temporal step. Therefore, if an oscillator receives a pulse from a firing neighbor which brings it above threshold, then it will only fire at the next time step. As a consequence, synchronous oscillators do not fire at the same time in our case but with a delay of the length of the time step, from the first one to the next. This produces an artificial migration rate in space, $V = dx/dt$, where dx and dt are the space and time steps, respectively. We try to loosely scale this velocity to match realistic values of slow-slip migration, $V = 13.3$ km/day.

We include a random heterogeneity of leakage rate α, using a centered, normally distributed noise with standard variation σ_α. Variations of α affect the period of firing of individual synthetic tremor sources—the higher α, the longer the period. This generates an intrinsic segmentation of synchronization in the system, as locally faster oscillators set the pace for their segment neighbors. This feature of the model is meant to simulate intrinsic factors that limit the size of synchronous bursts of tremor. It thus produces a segmentation of tremor activity from internal factors, which external perturbations from earthquakes must outweigh to be a major segmentation force.

External perturbations from earthquakes are modeled as randomly occurring pulses occurring at the position of an oscillator i, only affecting this given oscillator. A perturbation pulse adds a random stress increment to the local oscillator, with an intensity sampled from a normal distribution with mean 0 and standard variation $p/20$. Perturbations at a given location i follow a Poissonian law of occurrence with a rate of λ. The rate of perturbation varies in space, so that we can analyze the effects on segmentation of having more or less perturbation. We scale the rate of perturbation to 0 to 3000 perturbations/year to resemble the perturbation rates we measured in real tremor zones. In the simulation's case, however, only perturbations at the location of the source might trigger it. Figure S12 shows how the activity of one system differs when perturbed or not. Table S1 lists parameters of the model and the values used in the simulations presented here.

At each time step in the numerical scheme, (i) oscillators incrementally load, (ii) some are externally perturbed, (iii) they fire when above threshold, and lastly, (iv) they receive the stress pulse from firing neighbors. A catalog of oscillator firing events and perturbations is logged, to represent synthetic tremor events and nearby earthquake activity respectively.

Supplementary Materials

This PDF file includes:
Supplementary Text
Figs. S1 to S12
Table S1

REFERENCES AND NOTES

1. K. Obara, Nonvolcanic deep tremor associated with subduction in southwest Japan. *Science* **296**, 1679–1681 (2002).
2. G. Rogers, H. Dragert, Episodic tremor and slip on the Cascadia subduction zone: The chatter of silent slip. *Science* **300**, 1942–1943 (2003).
3. K. Obara, H. Hirose, Non-volcanic deep low-frequency tremors accompanying slow slips in the southwest Japan subduction zone. *Tectonophysics* **417**, 33–51 (2006).
4. K. Hall, D. Schmidt, H. Houston, Peak tremor rates lead peak slip rates during propagation of two large slow earthquakes in Cascadia. *Geochem. Geophys. Geosyst.* **20**, 4665–4675 (2019).
5. C. Villafuerte, V. M. Cruz-Atienza, Insights into the causal relationship between slow slip and tectonic tremor in Guerrero, Mexico. *J. Geophys. Res. Solid Earth* **122**, 6642–6656 (2017).
6. N. M. Bartlow, L. M. Wallace, R. J. Beavan, S. Bannister, P. Segall, Time-dependent modeling of slow slip events and associated seismicity and tremor at the Hikurangi subduction zone, New Zealand. *J. Geophys. Res. Solid Earth* **119**, 734–753 (2014).
7. W. B. Frank, E. E. Brodsky, Daily measurement of slow slip from low-frequency earthquakes is consistent with ordinary earthquake scaling. *Sci. Adv.* **5**, eaaw9386 (2019).
8. J. J. Clague, Evidence for large earthquakes at the Cascadia subduction zone. *Rev. Geophys.* **35**, 439–460 (1997).
9. M. Ando, Source mechanisms and tectonic significance of historical earthquakes along the nankai trough, Japan. *Tectonophysics* **27**, 119–140 (1975).
10. D. R. Shelly, G. C. Beroza, S. Ide, Non-volcanic tremor and low-frequency earthquake swarms. *Nature* **446**, 305–307 (2007).
11. K. Masuda, S. Ide, K. Ohta, T. Matsuzawa, Bridging the gap between low-frequency and very-low-frequency earthquakes. *Earth Planets Space* **72**, 47 (2020).
12. M. R. Brudzinski, R. M. Allen, Segmentation in episodic tremor and slip all along Cascadia. *Geology* **35**, 907–910 (2007).
13. G. Farge, C. Jaupart, W. B. Frank, N. M. Shapiro, Along-strike segmentation of seismic tremor and its relationship with the hydraulic structure of the subduction fault zone. *J. Geophys. Res. Solid Earth* **128**, e2023JB027584 (2023).
14. J. Maury, S. Ide, V. M. Cruz-Atienza, V. Kostoglodov, Spatiotemporal variations in slow earthquakes along the Mexican subduction zone. *J. Geophys. Res. Solid Earth* **123**, 1559–1575 (2018).
15. C. H. Scholz, Large earthquake triggering, clustering, and the synchronization of faults. *Bull. Seismol. Soc. Am.* **100**, 901–909 (2010).
16. D. R. Shelly, Z. Peng, D. P. Hill, C. Aiken, Triggered creep as a possible mechanism for delayed dynamic triggering of tremor and earthquakes. *Nat. Geosci.* **4**, 384–388 (2011).
17. R. Nakata, N. Suda, H. Tsuruoka, Non-volcanic tremor resulting from the combined effect of Earth tides and slow slip events. *Nat. Geosci.* **1**, 676–678 (2008).
18. M. Miyazawa, J. Mori, Evidence suggesting fluid flow beneath Japan due to periodic seismic triggering from the 2004 Sumatra-Andaman earthquake. *Geophys. Res. Lett.* **33**, L05303 (2006).
19. J. L. Rubinstein, M. La Rocca, J. E. Vidale, K. C. Creager, A. G. Wech, Tidal modulation of nonvolcanic tremor. *Science* **319**, 186–189 (2008).
20. J. L. Rubinstein, J. E. Vidale, J. Gomberg, P. Bodin, K. C. Creager, S. D. Malone, Non-volcanic tremor driven by large transient shear stresses. *Nature* **448**, 579–582 (2007).
21. D. R. Shelly, K. M. Johnson, Tremor reveals stress shadowing, deep postseismic creep, and depth-dependent slip recurrence on the lower-crustal San Andreas fault near Parkfield. *Geophys. Res. Lett.* **38**, L13312 (2011).
22. N. J. Van Der Elst, A. A. Delorey, D. R. Shelly, P. A. Johnson, Fortnightly modulation of San Andreas tremor and low-frequency earthquakes. *Proc. Natl. Acad. Sci. U.S.A.* **113**, 8601–8605 (2016).
23. J. Han, J. E. Vidale, H. Houston, K. Chao, K. Obara, Triggering of tremor and inferred slow slip by small earthquakes at the Nankai subduction zone in southwest Japan. *Geophys. Res. Lett.* **41**, 8053–8060 (2014).
24. A. G. Wech, Extending Alaska's plate boundary: Tectonic tremor generated by Yakutat subduction. *Geology* **44**, 587–590 (2016).
25. G. S. Fuis, T. E. Moore, G. Plafker, T. M. Brocher, M. A. Fisher, W. D. Mooney, W. J. Nokleberg, R. A. Page, B. C. Beaudoin, N. I. Christensen, A. R. Levander, W. J. Lutter, R. W. Saltus, N. A. Ruppert, Trans-Alaska Crustal Transect and continental evolution involving subduction underplating and synchronous foreland thrusting. *Geology* **36**, 267–270 (2008).
26. R. E. Mirollo, S. H. Strogatz, Synchronization of pulse-coupled biological oscillators. *SIAM J. Appl. Math.* **50**, 1645–1662 (1990).
27. R. Burridge, L. Knopoff, Model and theoretical seismicity. *Bull. Seismol. Soc. Am.* **57**, 341–371 (1967).
28. J. M. Carlson, J. S. Langer, Mechanical model of an earthquake fault. *Phys. Rev. A* **40**, 6470–6484 (1989).
29. Z. Olami, H. J. S. Feder, K. Christensen, Self-organized criticality in a continuous, nonconservative cellular automaton modeling earthquakes. *Phys. Rev. Lett.* **68**, 1244–1247 (1992).
30. Y. Ben-Zion, Episodic tremor and slip on a frictional interface with critical zero weakening in elastic solid: NVT-ETS and criticality. *Geophys. J. Int.* **189**, 1159–1168 (2012).
31. S. Ide, S. Yabe, Two-dimensional probabilistic cell automaton model for broadband slow earthquakes. *Pure Appl. Geophys.* **176**, 1021–1036 (2019).
32. K. Fukuda, T. Hatano, K. Mochizuki, Model for tectonic tremors: Enduring events, moment rate spectrum, and moment-duration scaling. *Phys. Rev. E* **105**, 014124 (2022).
33. H. M. Savage, C. Marone, Potential for earthquake triggering from transient deformations. *J. Geophys. Res. Solid Earth* **113**, B05302 (2008).
34. J. D. Kirkpatrick, Å. Fagereng, D. R. Shelly, Geological constraints on the mechanisms of slow earthquakes. *Nat. Rev. Earth Environ.* **2**, 285–301 (2021).
35. J. R. Leeman, C. Marone, D. M. Saffer, Frictional mechanics of slow earthquakes. *J. Geophys. Res. Solid Earth* **123**, 7931–7949 (2018).

36. J. Gomberg, M. L. Blanpied, N. M. Beeler, Transient triggering of near and distant earthquakes. *Bull. Seismol. Soc. Am.* **87**, 294–309 (1997).

37. H. Perfettini, J. Schmittbuhl, A. Cochard, Shear and normal load perturbations on a two-dimensional continuous fault: 2. Dynamic triggering. *J. Geophys. Res. Solid Earth* **108**, 2002JB001805 (2003).

38. N. J. Van Der Elst, H. M. Savage, Frequency dependence of delayed and instantaneous triggering on laboratory and simulated faults governed by rate-state friction. *J. Geophys. Res. Solid Earth* **120**, 3406–3429 (2015).

39. D. C. Boyarko, M. R. Brudzinski, Spatial and temporal patterns of nonvolcanic tremor along the southern Cascadia subduction zone. *J. Geophys. Res. Solid Earth* **115**, B00A22 (2010).

40. R. E. Wells, R. J. Blakely, A. G. Wech, P. A. McCrory, A. Michael, Cascadia subduction tremor muted by crustal faults. *Geology* **45**, 515–518 (2017).

41. M. G. Bostock, N. I. Christensen, S. M. Peacock, Seismicity in Cascadia. *Lithos* **332-333**, 55–66 (2019).

42. N. J. van der Elst, E. E. Brodsky, Connecting near-field and far-field earthquake triggering to dynamic strain. *J. Geophys. Res. Solid Earth* **115**, B07311 (2010).

43. A. R. Lowry, Resonant slow fault slip in subduction zones forced by climatic load stress. *Nature* **442**, 802–805 (2006).

44. A. Inbal, T. Cristea-Platon, J.-P. Ampuero, G. Hillers, D. Agnew, S. E. Hough, Sources of long-range anthropogenic noise in southern California and implications for tectonic tremor detection. *Bull. Seismol. Soc. Am.* **108**, 3511–3527 (2018).

45. C. Li, Z. Li, Z. Peng, C. Zhang, N. Nakata, T. Sickbert, Long-period long-duration events detected by the IRIS community wavefield demonstration experiment in Oklahoma: Tremor or train signals? *Seismol. Res. Lett.* **89**, 1652–1659 (2018).

46. W. B. Frank, N. M. Shapiro, A. L. Husker, V. Kostoglodov, A. Romanenko, M. Campillo, Using systematically characterized low-frequency earthquakes as a fault probe in Guerrero, Mexico. *J. Geophys. Res. Solid Earth* **119**, 7686–7700 (2014).

47. P. Romanet, S. Ide, Ambient tectonic tremors in Manawatu, Cape Turnagain, Marlborough, and Puysegur, New Zealand. *Earth Planets Space* **71**, 59 (2019).

48. S. Ide, Variety and spatial heterogeneity of tectonic tremor worldwide. *J. Geophys. Res. Solid Earth* **117**, B03302 (2012).

49. K. Chao, Z. Peng, W. B. Frank, G. A. Prieto, K. Obara, Isolated triggered tremor spots in South America and implications for global tremor activity. *Seismol. Res. Lett.* **90**, 1726–1739 (2019).

50. A. Gallego, R. M. Russo, D. Comte, V. Mocanu, R. E. Murdie, J. C. VanDecar, Tidal modulation of continuous nonvolcanic seismic tremor in the Chile triple junction region. *Geochem. Geophys. Geosyst.* **14**, 851–863 (2013).

51. S. Ide, K. H. Chen, Spatiotemporal characteristics of tectonic tremors in the collisional orogen of Taiwan. *Geophys. Res. Lett.* **51**, e2023GL106759 (2024).

52. W. M. Behr, R. Bürgmann, What's down there? The structures, materials and environment of deep-seated slow slip and tremor. *Philos. Trans. R. Soc. Math. Phys. Eng. Sci.* **379**, 20200218 (2021).

53. W. B. Frank, Slow slip hidden in the noise: The intermittence of tectonic release. *Geophys. Res. Lett.* **43**, 10,125–10,133 (2016).

54. W. B. Frank, N. M. Shapiro, A. L. Husker, V. Kostoglodov, A. A. Gusev, M. Campillo, The evolving interaction of low-frequency earthquakes during transient slip. *Sci. Adv.* **2**, e1501616 (2016).

55. N. Poiata, J.-P. Vilotte, N. M. Shapiro, M. Supino, K. Obara, Complexity of deep low-frequency earthquake activity in Shikoku (Japan) imaged from the analysis of continuous seismic data. *J. Geophys. Res. Solid Earth* **126**, e2021JB022138 (2021).

56. G. Farge, Notebooks for reproducing "The Big Impact of Small Quakes on Tectonic Tremor Synchronization," version v1.0, Zenodo (2025); https://doi.org/10.5281/ZENODO.14722432.

57. T. Nishikawa, S. Ide, T. Nishimura, A review on slow earthquakes in the Japan Trench. *Prog. Earth Planet. Sci.* **10**, 1 (2023).

58. M. Kano, N. Aso, T. Matsuzawa, S. Ide, S. Annoura, R. Arai, S. Baba, M. Bostock, K. Chao, K. Heki, S. Itaba, Y. Ito, N. Kamaya, T. Maeda, J. Maury, M. Nakamura, T. Nishimura, K. Obana, K. Ohta, N. Poiata, H. Rousset, H. Sugioka, R. Takagi, T. Takahashi, A. Takeo, Y. Tu, N. Uchida, Y. Yamashita, K. Obara, Development of a slow earthquake database. *Seismol. Res. Lett.* **89**, 1566–1575 (2018).

59. T. Iwasaki, H. Sato, T. Ishiyama, M. Shinohara, A. Hashima, "Fundamental structure model of island arcs and subducted plates in and around Japan" in *AGU Fall Meeting Abstracts* (2015), vol. 2015, pp. T31B-2878. https://ui.adsabs.harvard.edu/abs/2015AGUFM.T31B2878I.

60. T. Maeda, K. Obara, Spatiotemporal distribution of seismic energy radiation from low-frequency tremor in western Shikoku, Japan. *J. Geophys. Res. Solid Earth* **114**, 2008JB006043 (2009).

61. K. Obara, S. Tanaka, T. Maeda, T. Matsuzawa, Depth-dependent activity of non-volcanic tremor in southwest Japan. *Geophys. Res. Lett.* **37**, 2010GL043679 (2010).

62. K. Idehara, S. Yabe, S. Ide, Regional and global variations in the temporal clustering of tectonic tremor activity. *Earth Planets Space* **66**, 66 (2014).

63. A. G. Wech, Cataloging tectonic tremor energy radiation in the Cascadia subduction zone. *J. Geophys. Res. Solid Earth* **126**, e2021JB022523 (2021).

64. G. Hayes, Slab2 - A Comprehensive Subduction Zone Geometry Model, U.S. Geological Survey (2018); https://doi.org/10.5066/F7PV6JNV.

65. E. K. Todd, S. Y. Schwartz, Tectonic tremor along the northern Hikurangi Margin, New Zealand, between 2010 and 2015. *J. Geophys. Res. Solid Earth* **121**, 8706–8719 (2016).

66. D. Shelly, An Updated Catalog of Low-Frequency Earthquakes Along the San Andreas Fault Near Parkfield, California, U.S. Geological Survey (2024); https://doi.org/10.5066/P13CPJFU.

67. D. R. Shelly, A 15 year catalog of more than 1 million low-frequency earthquakes: Tracking tremor and slip along the deep San Andreas Fault. *J. Geophys. Res. Solid Earth* **122**, 3739–3753 (2017).

68. F. Waldhauser, D. P. Schaff, Large-scale relocation of two decades of Northern California seismicity using cross-correlation and double-difference methods. *J. Geophys. Res. Solid Earth* **113**, B08311 (2008).

69. F. Waldhauser, Near-real-time double-difference event location using long-term seismic archives, with application to Northern California. *Bull. Seismol. Soc. Am.* **99**, 2736–2748 (2009).

70. S. Ide, Tectonic tremors in Taiwan, Zenodo (2023); https://doi.org/10.5281/ZENODO.10400863.